# Photophysical Properties of Aromatic and Antiaromatic Porphyrinoids

**14th, April 2011**

**Principal Investigators:** Prof. Dongho Kim

**E-mail Address**: dongho@yonsei.ac.kr

**Institution**: Spectroscopy Laboratory for Functional π-Electronic Systems and

Department of Chemistry, Yonsei University, Seoul 120-749, Korea

**Mailing Address**: 134 Shinchon-dong, Seodaemun-gu, Seoul 120-749, Korea

**Phone**: +82-2-2123-2436

**Fax**: +82-2-2123-2434

**Period of Performance**: 16/05/2010 – 15/05/2011

# Report Documentation Page

*Form Approved*
*OMB No. 0704-0188*



| 1. REPORT DATE | 2. REPORT TYPE | 3. DATES COVERED |
|---|---|---|
| **19 APR 2011** | **FInal** | **29-04-2010 to 28-04-2011** |

4. TITLE AND SUBTITLE
**Photophysical Properties of Aromatic and Antiaromatic Porphyrinoids**

5a. CONTRACT NUMBER
**FA23861014080**

5b. GRANT NUMBER

5c. PROGRAM ELEMENT NUMBER

6. AUTHOR(S)
**Dongho Kim**

5d. PROJECT NUMBER

5e. TASK NUMBER

5f. WORK UNIT NUMBER

7. PERFORMING ORGANIZATION NAME(S) AND ADDRESS(ES)
**Yonsei University,Shinchon-Dong 134, Seodaemoon-Ku,Seoul 120-749,Korea (South),TW,120-749**

8. PERFORMING ORGANIZATION REPORT NUMBER
**N/A**

9. SPONSORING/MONITORING AGENCY NAME(S) AND ADDRESS(ES)
**AOARD, UNIT 45002, APO, AP, 96337-5002**

10. SPONSOR/MONITOR'S ACRONYM(S)
**AOARD**

11. SPONSOR/MONITOR'S REPORT NUMBER(S)
**AOARD-104080**

12. DISTRIBUTION/AVAILABILITY STATEMENT
**Approved for public release; distribution unlimited**

13. SUPPLEMENTARY NOTES

14. ABSTRACT
**This is the report of an investigation of the photophysical properties of various H?ckel or M?bius (anti)aromatic porphyrinoids such as expanded porphyrins, porphycenes, etc. using theoretical calculations and various spectroscopic methodologies in conjunction with the topology transformation between aromatic and antiaromatic porphyrinoids by conformational control vial solvent change and redox chemistry.**

15. SUBJECT TERMS
**Materials Characterization, Materials Chemistry, Nonlinear Optical Materials, Spectroscopy**

| 16. SECURITY CLASSIFICATION OF: | | | 17. LIMITATION OF ABSTRACT | 18. NUMBER OF PAGES | 19a. NAME OF RESPONSIBLE PERSON |
|---|---|---|---|---|---|
| a. REPORT | b. ABSTRACT | c. THIS PAGE | | | |
| **unclassified** | **unclassified** | **unclassified** | **Same as Report (SAR)** | **20** | |

# Table of Contents

## Abstract

In this report for AFSOR/AOARD project (*FA2386-10-1-4080*), we have investigated the photophysical properties of various Hückel or Möbius (anti)aromatic porphyrinoids such as expanded porphyrins, porphycenes *etc*. using theoretical calculations and various spectroscopic methodologies in conjunction with the topology transformation between aromatic and antiaromatic porphyrinoids by conformational control via solvent change and redox chemistry, *etc*.


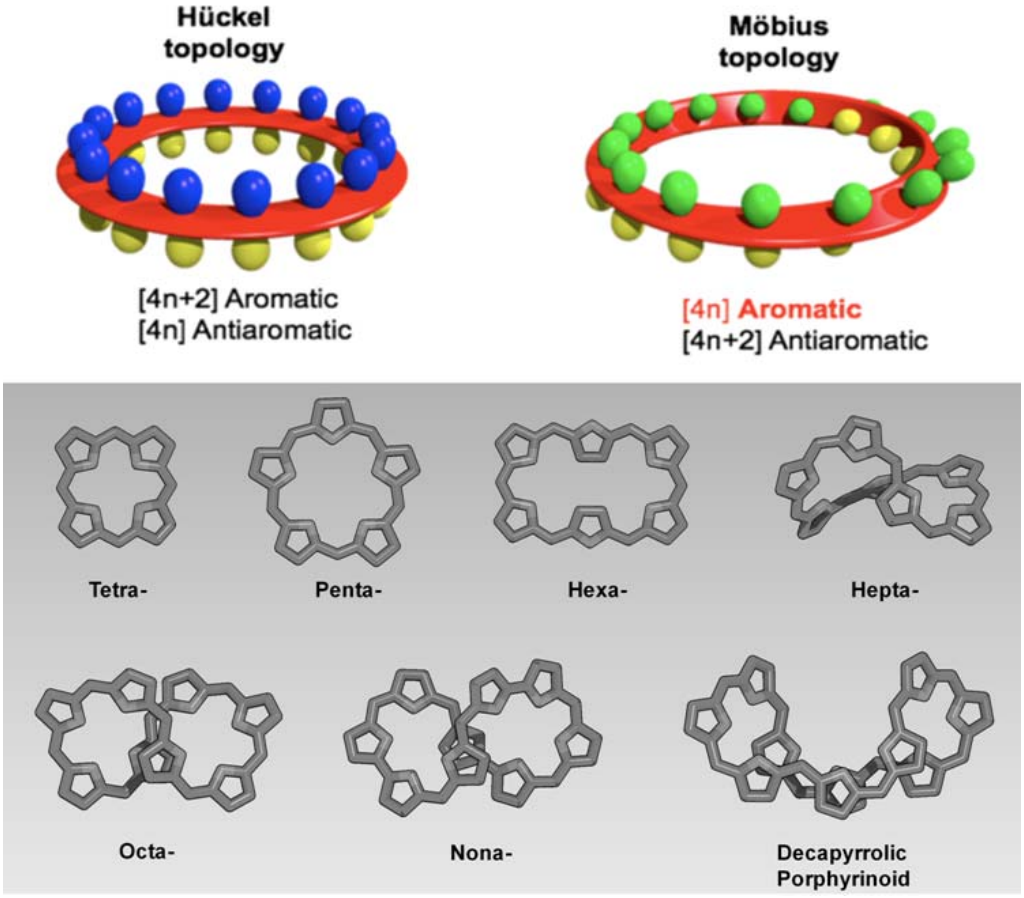


**Figure 1.** Hückel and Möbius aromaticity (top) and schematic molecular structures of various porphyrinoids (bottom).

# Introduction

Aromaticity is regarded as one of the most important concepts in modern chemistry. Although the history of this concept began with the discovery of benzene by Faraday in 1825, there is no simple definition to explain what the aromaticity really is. Most widely-accepted notion is that cyclic conjugated molecular systems with [4n+2]π-electrons have closed-shell electron configurations and reveal aromaticity like benzene. This is known as Hückel's rule. In contrast to the fact that Hückel considered the planar molecular structure, Heilbronner suggested that [4n]π-electron conjugated system can have a closed-shell configuration, namely aromatic property, when the system takes Möbius strip-like topology with a half-twisted π surface in the π-conjugated pathways. This is the key concept of Möbius aromaticity, in which Hückel's rule is adopted inversely; [4n]π-systems are aromatic but those with [4n+2]π-electrons are antiaromatic.

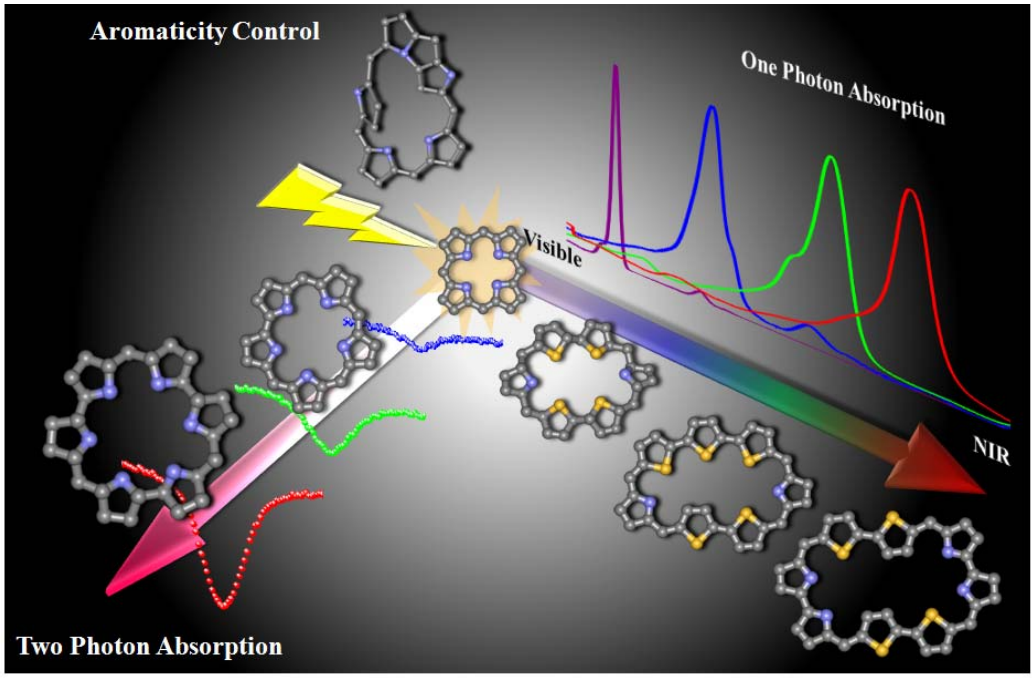


**Figure 2.** Photophysical properties of various porphyrinoids.

Porphyrins and their analogues (porphyrinoids) are particularly attractive molecules for exploration of various types of aromaticity, because most porphyrinoids possess circular conjugation pathways in their macrocyclic ring with various molecular structures (**Figure 2**). π-electron delocalization and aromaticity in porphyrinoids are strongly affected by i) structural modifications, ii) redox chemistry, and iii) NH-tautomerization process, etc.

Furthermore, this aromaticity has a strong influence on the spectroscopic properties and chemical reactivity of porphyrinoids. In this context, considerable efforts have been devoted to exploring and understanding relationship between aromaticity and spectroscopic properties in a variety of aromatic and antiaromatic porphyrinoids.

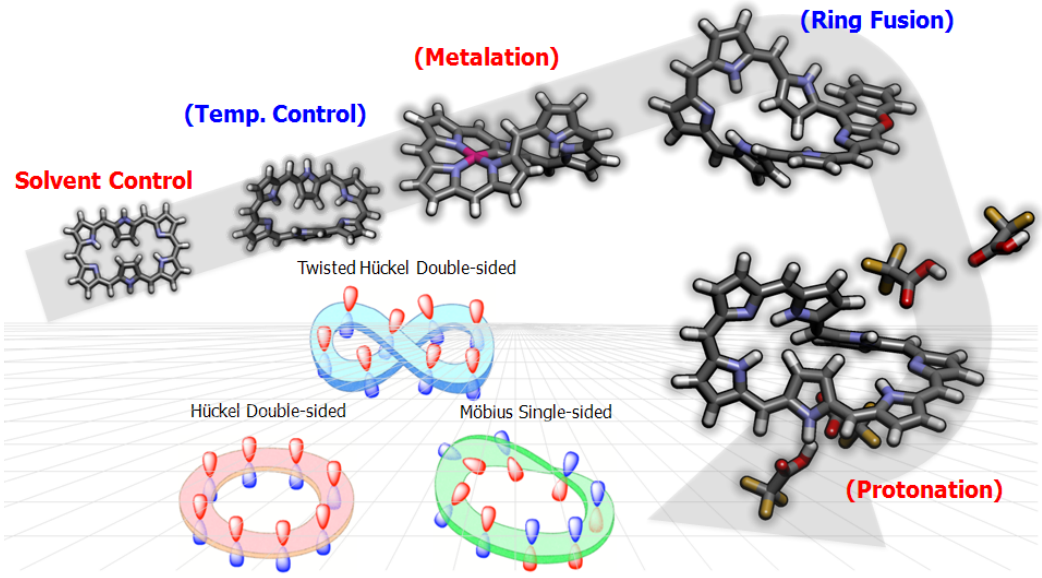


**Figure 3.** Examples of aromaticity control for expanded porphryins

Thus, a series of various porphyrinoids are in the limelight being expected to shed light on this field because they have some advantages to study the aromaticity; i) it is possible to control the number of conjugated π-electrons by changing the number of connected pyrrole rings, ii) by providing a comparable set of [4n]/[4n+2] molecular systems through a facile two-electron reduction/oxidation process, the systematic investigations are easily accessible, satisfying the prerequisites that only the number of π-electrons has to be different with the same structure and chemical environment, and iii) above all, it is easy to change the molecular conformations by both synthetic and non-synthetic ways. Again, it should be noted that the topology control is an important factor in assessing the structure-property relationship. In this regard, various attempts to modify the overall structures of porphyrinoids have been made by temperature control, solvent changes, and functional group modifications (**Figure 3**). With these active control methods of molecular topologies in hand, the structure-property relationship of porphyrinoids in conjunction with aromaticity has been vigorously explored by using ultrafast spectroscopic measurements as well as theoretical calculations.

## Methodologies

### (1) Experimental Method

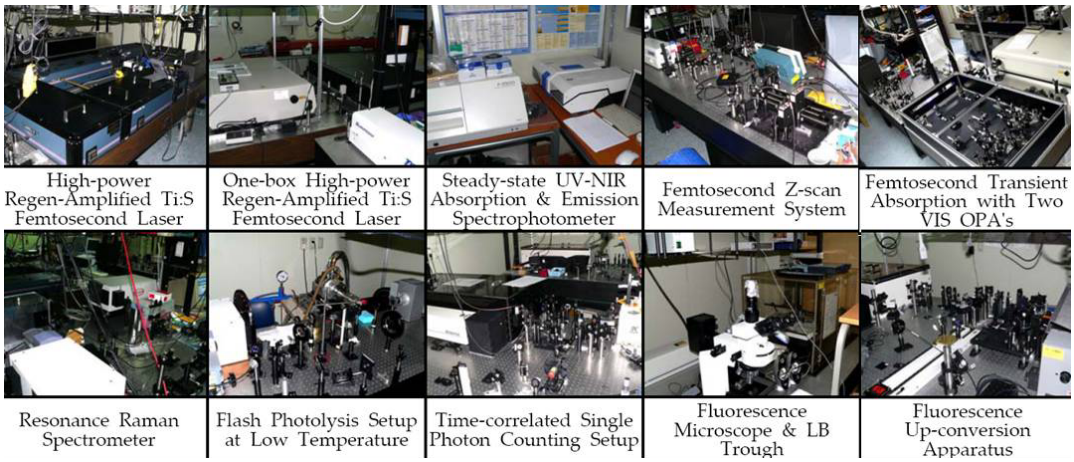


① **Steady-State Laser Spectroscopy**

- Laser-Induced Luminescence Spectroscopy
- Resonance Raman Spectroscopy

② **Time-Resolved Laser Spectroscopy**

- Nanosecond Flash Photolysis
- Picosecond Time-Correlated Single Photon Counting (TCSPC) Method
- Vis/IR Femtosecond Transient Absorption Spectroscopy
- Femtosecond Fluorescence Up-Conversion Spectroscopy

③ **Non-Linear Spectroscopy**

- Femtosecond Z-Scan Method

### (2) Quantum Mechanical Calculation

- Nuclear-Independent Chemical Shift (**NICS**) Values
- Anisotropy of the Induced Current Density (**AICD**) Calculation
- Molecular Orbitals & Electronic Excited-State Excitation Energies

## Results and Discussion

### 1. **Investigation of Aromaticity and Photophysical Properties in [18]/[20]π Porphycenes**

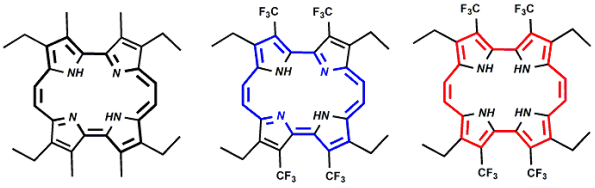


**Figure 4.** Schematic molecular structures of **[18]EtioPc**, **[18]$CF_3$Pc**, and **[20]$CF_3$Pc**.

Porphyrins and their analogues (porphyrinoids) are particularly attractive molecules for exploration of various types of aromaticity. Generally, porphyrinoids with [4n+2]π electrons in the main π-conjugation pathway usually reveal an obvious aromatic character. While these [4n+2]π porphyrinoids have been intensively synthesized and characterized, porphyrinoids with [4n]π electrons in their delocalized pathways have been little explored owing to their synthetic difficulties and instabilities in ambient condition. As a consequence, a majority of studies on [4n]π porphyrinoids have dealt with expanded porphyrins, because the difference in resonance stabilization energies between [4n]π and [4n+2]π electronic systems decreases for larger values of n. In this regard, the isolation and stability of [4n]π porphyrinoids are the essential requirements for the reliable photophysical characterization. In this project, we have investigated the relationship between aromaticity and photophysical properties of [18]/[20]π porphycenes (**[18]EtioPc**, **[18]$CF_3$Pc**, and **[20]$CF_3$Pc)** using theoretical calculations and spectroscopic methodologies (**Figure 4**).

**(1) Molecular Structures and MO Diagrams:** While the optimized molecular structure of **[18]EtioPc** reveals a quite planar geometry, **[18]$CF_3$Pc** shows a slightly ruffled structure due to the steric/electronic repulsion between bulky trifluoromethyl substituents (**Figure 5**). Furthermore, **[20]$CF_3$Pc** exhibits more distorted conformation than **[18]$CF_3$Pc** due to additional steric repulsion between inner hydrogen atoms inside the macrocycle.

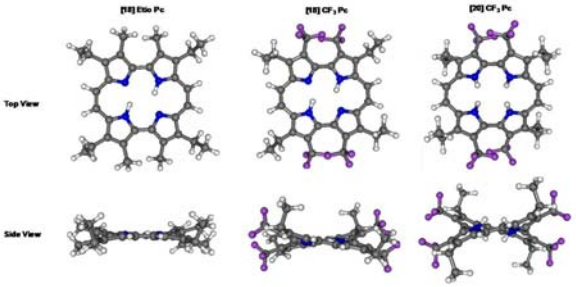


**Figure 5.** Optimized molecular structures of **[18]EtioPc**, **[18]$CF_3$Pc**, and **[20]$CF_3$Pc**.

Molecular orbital (MO) diagrams of **[18]EtioPc** reveal a general feature of aromatic porphycene, which shows nearly degenerate HOMO/HOMO-1 and a relatively large energy splitting between LUMO and LUMO+1 (1.26 eV) due to the reduced symmetry ($D_{2h}$) as

compared with its corresponding free-base porphyrin ($D_{4h}$). Although the MOs of **[18]CF$_3$Pc** also show a quite similar behavior to **[18]EtioPc**, the energy stabilization of LUMO was observed due to the existence of electron withdrawing substituents (**Figure 6**). Consequently, **[18]CF$_3$Pc** reveals the distinctly smaller HOMO-LUMO gap by 0.26 eV than **[18]EtioPc**. Especially, the HOMO-LUMO energy gap of **[20]CF$_3$Pc** is significantly increased to 2.96 eV as compared with 2.12 eV for **[18]CF$_3$Pc**.

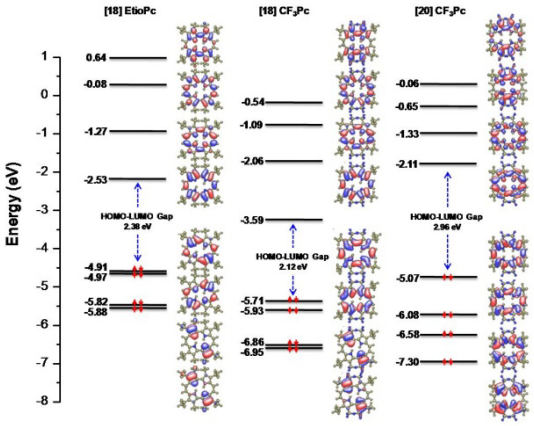


**Figure 6.** MO diagrams of **[18]EtioPc** (left), **[18]CF$_3$Pc** (center), and **[20]CF$_3$Pc** (right).

**(2) Aromaticity and Electron Delocalization:** To reveal the π-electron delocalization behaviors, we have investigated the diatropicity or paratropicity of three porphycene molecules by ACID plot analysis (**Figure 7**). As shown in **Figure 7**, the ACID plots of **[18]EtioPc** and **[18]CF$_3$Pc** reveal clear clockwise current density vectors, indicating a diamagnetic ring current. On the contrary, that of **[20]CF$_3$Pc** shows relatively weak counter-clockwise current flow, which means the induced paratropic ring current.

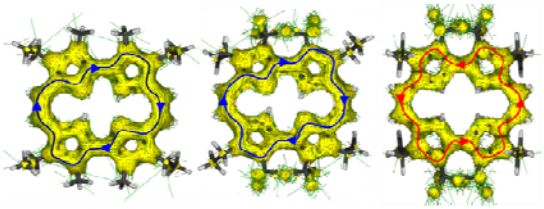

**Figure 7**. Induced current density maps of **[18]EtioPc** (left), **[18]CF$_3$Pc** (center), and **[20]CF$_3$Pc** (right). Red and blue lines indicate the main conjugation pathways.

Furthermore, the ring current density maps on [18]π porphycenes and [20]π porphycene show a prominent difference upon changing the isosurface values in ACID plots (**Figure 8**). Although **[18]EtioPc** and **[18]CF$_3$Pc** reveal continuous boundary surface enclosing the delocalized electrons even at the isosurface values of 0.091 and 0.078, respectively, **[20]CF$_3$Pc** does not show a continuous

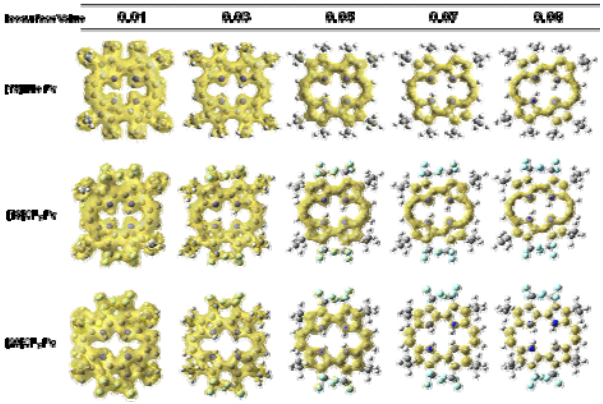

**Figure 8.** Current density maps of **[18]EtioPc**, **[18]CF$_3$Pc**, and **[20]CF$_3$Pc**.

current density above the isosurface value of 0.051. This difference between [18] and [20] porphycenes indicates that π-electron delocalization is more effective in two [18]π porphycenes than **[20]CF$_3$Pc**.

The NICS(0) values of **[18]EtioPc** and **[18]CF$_3$Pc** have been estimated to be large negative ones, -13.4 and -12.4, respectively. In contrast, **[20]CF$_3$Pc** shows positive NICS(0) value of +4.7 at the center of macrocycle. According to these results, we think that two [18]π porphycenes reveal an obvious aromatic character. Meanwhile, the absolute NICS value of **[20]CF$_3$Pc** is noticeably smaller than those of two aromatic [18]π porphycenes, which means that the strength of the paratropic ring current of **[20]CF$_3$Pc** is relatively weaker than that of the diatropic ring current of two aromatic [18]π porphycenes. Based on these results, we suggest that **[20]CF$_3$Pc** reveals moderately antiaromatic character due to its distorted structure.

**(3) Photophysical Properties:** Aromatic [18]π porphycenes show general features of free-base [18]π porphyrinoids in the steady-state spectra, which exhibits intense Soret band, split Q-bands and well-structured fluorescence spectra (**Figure 9**). Particularly, **[18]CF$_3$Pc** exhibits a bathochromic shift of Q-bands and slightly larger Stokes shift as compared with **[18]EtioPc**. Furthermore, to investigate the excited-state dynamics and non-linear optical properties of [**18]EtioPc** and **[18]CF$_3$Pc**, we have carried out time-correlated single photon counting (TCSPC), nanosecond flash photolysis, and femtosecond Z-scan measurements in toluene.

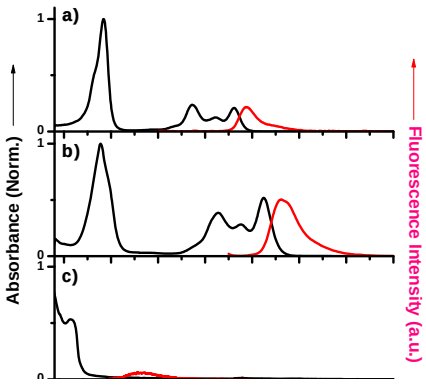


**Figure 9.** Steady-state absorption (black line) and fluorescence spectra (red line) of **[18]EtioPc** (a), **[18]CF$_3$Pc** (b), and **[20]CF$_3$Pc** (c) in toluene.

The decay profiles of [**18]EtioPc** and **[18]CF$_3$Pc** can be fitted to a single exponential function with the time constants of 296 and 30 μs, respectively. Additionally, the fluorescence temporal profiles of [**18]EtioPc** and **[18]CF$_3$Pc** reveal single exponential decay behaviors, with the lifetime of 3.92 and 1.08 ns, respectively. Also, **[18]CF$_3$Pc** exhibits the TPA cross-section value of 1820 GM, which is slightly smaller than that of **[18]EtioPc** (2150 GM) (**Figure 10).**

Obviously, compared with planar **[18]EtioPc**, distorted **[18]CF$_3$Pc** shows distinctive photophysical behaviors such as i) bathochromic shift of Q-bands, ii) much shorter excited singlet- and triplet-state lifetimes, and iii) slightly smaller TPA value, etc. The origin of these distinctive features of **[18]CF$_3$Pc** can be understood in terms of an interplay between reduced HOMO-LUMO gap and structural distortion of **[18]CF$_3$Pc**.

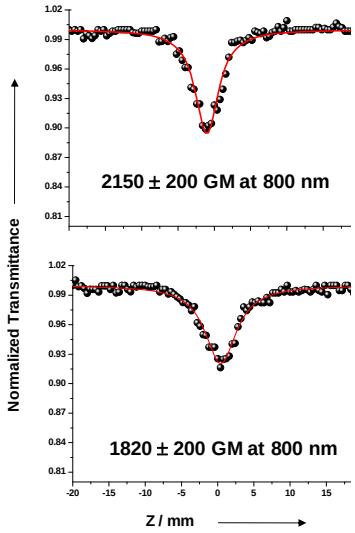


**Figure 10.** Z-Scan curve traces of **[18]EtioPc** (top) and **[18]$CF_3$Pc** (bottom) at 800 nm

Noticeably, compared with two aromatic porphycenes, antiaromatic **[20]$CF_3$Pc** exhibits quite different features in the steady state spectra and excited state dynamics. **[20]$CF_3$Pc** shows intense band at 321 nm and very weak and broad band at around 400 nm in the absorption spectrum. Although these absorption features of **[20]$CF_3$Pc** seem to be similar to those of [4n]π porphyrinoids without Q-bands, there are obvious differences between [20]π porphycenes and other [4n]π porphyrinoids.

The most [4n]π porphyrinoids have much smaller HOMO-LUMO gaps than their corresponding [4n+2]π porphyrinoids. These electronic features of [4n]π porphyrinoid systems with small HOMO-LUMO gaps are responsible for the NIR optically dark state absorption, a lack of fluorescence, and very short excited-state lifetime. However, the HOMO-LUMO gap of **[20]$CF_3$Pc** is relatively larger than that of aromatic **[18]$CF_3$Pc**. Moreover, the calculated vertical transition energy for the lowest excited state of **[20]$CF_3$Pc** is estimated to be energetically higher than that of **[18]$CF_3$Pc**. Furthermore, we have also observed weak fluorescence spectrum of **[20]$CF_3$Pc** at 475 nm, which is in a sharp contrast with non-fluorescent behaviors of antiaromatic [4n]π porphyrinoids.

The origin of this contrasting feature of [20]π porphycene arises from a uniquely large energy splitting between LUMO and LUMO+1 of [18]π porphycene with $D_{2h}$ symmetry as compared with other aromatic [4n+2]π porphyrinoids with nearly degenerate LUMO/LUMO+1. When two electrons are filled into the LUMO level of aromatic [4n+2]π porphyrinoid, the LUMO level should be stabilized and act as the HOMO level of [4n]π porphyrinoid. Thus, the HOMO-LUMO energy gap of [4n]π porphyrinoid is sensitive to the energy difference between LUMO and LUMO+1 of its corresponding [4n+2]π porphyrinoid (**Figure 11**).

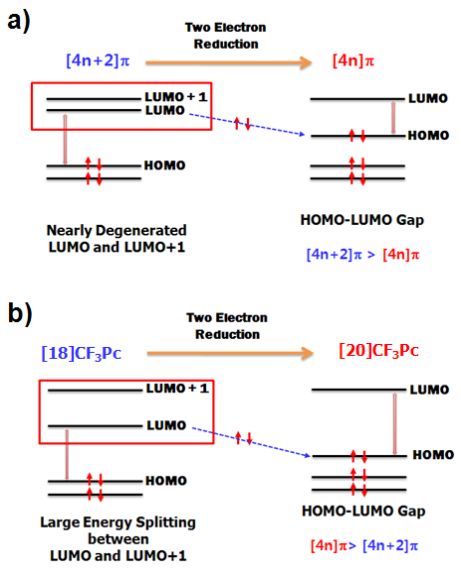


**Figure 11.** Schematic energy level diagram differences of typical [4n]/[4n+2] porphyrinoids with degenerated LUMO and LUMO+1 (a) and [18]/[20]$CF_3$Pc (b).

## 2. Solvent Dependent Aromatic versus Antiaromatic Conformational Switching

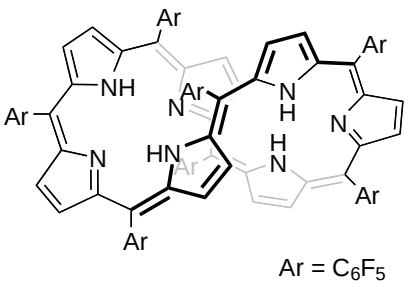


**Figure 12.** Schematic molecular structure of [32]heptaphyrin

We have investigated solvent dependent conformational changes and subsequent photophysical properties of *meso*-(heptakis)pentafluorophenyl [32] heptaphyrin (**Figure 12**). In this study, by performing the femtosecond time-resolved transient absorption (TA) spectroscopy and global analysis, we have resolved complicated conformational dynamics in solution by detecting characteristic spectroscopic features of aromatic, nonaromatic, and antiaromatic expanded porphyrins with their structural topologies.

**(1) Steady-State Absorption Spectra:** In toluene, the absorption spectra exhibit a relatively broad B-like band at 600 nm without any Q-like bands in NIR region. In ethyl ether, a broad and split B-like band is observed at 590 and 637 nm, and very weak Q-like bands are observed in the region of 800~1000 nm. In THF, however, a sharp and intense B-like band is observed at 646 nm with a shoulder at 687 nm, and Q-like bands in NIR region are clearly observed in contrast with very weak and featureless Q-like bands in ethyl ether. These changes in spectral features are further remarkable in DMSO (**Figure 13**).

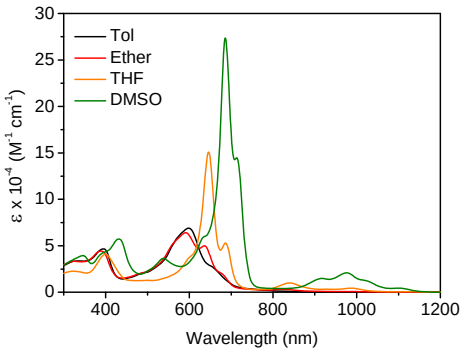


**Figure 13.** Steady-state absorption and fluorescence (inset) spectra of [32]heptaphyrin in various solvents measured at room temperature

The absorption spectrum in DMSO can be assigned to a twisted Möbius aromatic conformer by referring that in our previous observations, and ill-defined spectra in toluene and ethyl ether can be interpreted in terms of the formation of antiaromatic species on the basis of the related studies. Therefore, it is suggested that increase in solvent polarity induces the conformational changes of [32]heptaphyrin from antiaromatic to aromatic species.

**(2) Excited-State Dynamics:** The TA spectra in toluene show broad ground-state bleach (GSB) signals at 600 nm with strong excited-state absorption (ESA) signals around 700 nm (**Figure 14**). Through the global analysis, two decay associated spectra have been extracted. The decay associated spectrum at early time-evolution reveals broad and red-shifted ESA

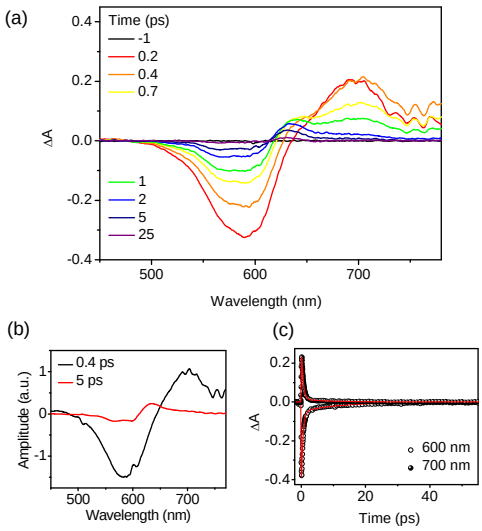


**Figure 14**. (a) Femtosecond transient absorption spectra, (b) decay associated spectra, and (c) temporal profiles of [32]heptaphyrin in toluene measured at room temperature.

signals whereas the spectrum at longer time-evolution shows blue-shifted ESA signals. These two spectra indicate the TA spectra before and after vibrational relaxation process, respectively, not those of two different conformers. The decay profiles probed at 600 and 700 nm were fitted by two exponential functions and the time constants were 0.4 and 5 ps, respectively. The shorter time constant of less than 1 ps is attributed to the vibrational energy relaxation process, and thus the lowest singlet excited-state lifetime can be estimated to be 5 ps in toluene. This short-lived singlet excited-state lifetime is consistent with the non-fluorescent behavior in toluene.

On the contrary, the TA spectra measured in THF show sharp and intense GSB signals at 650 and 690 nm, and the intensity of ESA signals at around 610 nm is relatively weak compared to that of GSB signals (**Figure 15**). Also, there is no band shifts with an increase in the delay time. In the global analysis, only one decay associated spectrum was found, indicating that there is one depopulation process or conformer. In line with this, the decay profiles at 614 and 648 nm were fitted by single exponential function with the time constant of 65 ps.

The TA spectra measured in ethyl ether exhibit more complicated aspects (**Figure 16**). Upon photoexcitation at 640 nm, broad GSB signals at 590 nm, sharp GSB signals at 640 nm, and strong ESA bands at around 700 nm appear at the initial time delay. As the delay time increases, both GSB at 590 nm and ESA at 700 nm decay very quickly while GSB at 640 nm disappears slowly with an appearance of ESA bands at 610 nm and weak GSB bands at 690 nm. Three different TA spectra were extracted from the global

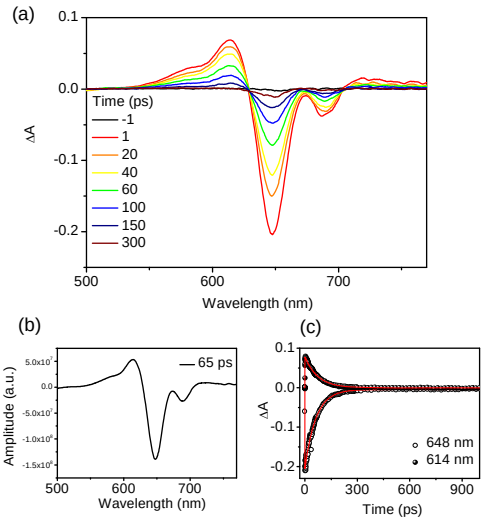


**Figure 15.** (a) Femtosecond transient absorption spectra, (b) decay associated spectra, and (c) temporal profiles of [32]heptaphyrin in THF measured at room temperature.

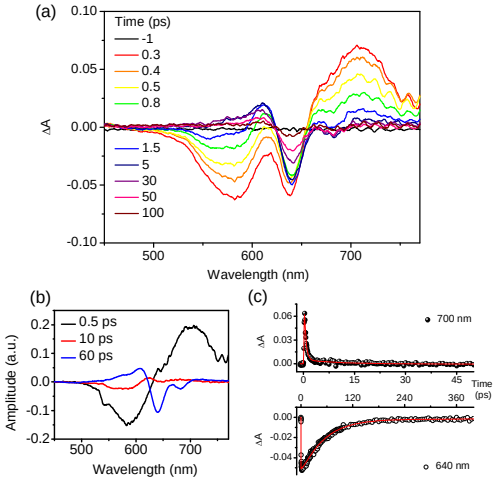


**Figure 16.** (a) Femtosecond transient absorption spectra, (b) decay associated spectra, and (c) temporal profiles of [32]heptaphyrin in ethyl ether measured at room temperature.

analysis. Since the decay associated spectra with the time constants of 0.5 and 10 ps have the same spectral shapes as those in toluene, we could conclude that these two spectra are originated from the molecular species existing in toluene. In contrast, the decay associated spectrum with the time constant of 60 ps exhibits the same spectral shape as that in THF, implying that this spectrum is contributed by the molecular species existing in THF. Moreover, the two time constants of 10 and 60 ps were also estimated in the decay profile probed at 640 nm. Each component is respectively consistent with the lowest singlet excited-state lifetimes in toluene and THF, providing us with strong evidence on our assumption that there are two different conformers, denoted as **toluene–conformer** and **THF–conformer**, in ethyl ether. In the decay profile probed at 700 nm, however, only the time constants of 0.5 and 10.0 ps originating from **toluene–conformer** were obtained because the contribution of **THF–conformer** to the decay dynamics is negligible in this wavelength region as shown in its decay associated spectra.

**(3) Aromaticity of Toluene– and THF–Conformers:** By using the anisotropy of the induced current density (AICD) and nucleus independent chemical shift (NICS) calculations, the degrees of aromaticity in the two conformers were quantitatively examined (**Figure 17**). As shown in **Figure 17a,** the current density vectors of **toluene–conformer** indicate counter-clockwise overall currents when we look toward the upper side sitting at the bottom of the molecule (against the direction of magnetic field vector), which means paratropic ring currents and antiaromaticity. However, the current density vectors of

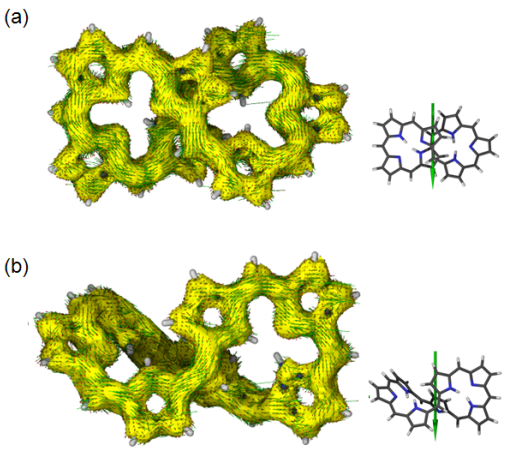


**Figure 17.** AICD plots of (a) figure-eight-like and (b) Möbius strip-like structures of [32]heptaphyrin.

**THF–conformer** show clockwise currents, which indicate diatropic ring currents and aromaticity. It is quite impressive that in AICD calculations the same molecule can exhibit the opposite ring currents depending on the structures even though the structural differences do not seem to be large. Moreover, the commonly used indices of aromaticity, NICS values were calculated as +7.1 ppm for **toluene–conformer** and -10.8 ppm for **THF–conformer**, supporting their aromatic characters (positive value means antiaromaticity and negative value indicates aromaticity). These results imply that a little change in conformation can cause a huge difference in molecular aromaticity and its electronic nature. The variation of solvent polarity will be enough to trigger such a small conformational change.

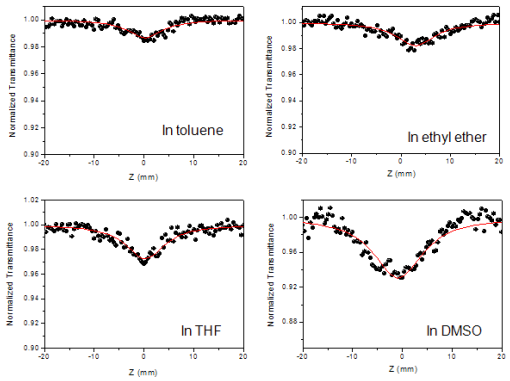


**Figure 18.** Z-scan curves of [32]heptaphyrin in various solvents measured at room temperature

The TPA cross section values in four different solvents also reflected the change of aromaticity. The TPA values of [32]heptaphyrin increased from 2000 GM to 2200, 3100, and 4700 GM as the solvents were changed from toluene to ethyl ether, THF, and DMSO, respectively (**Figure 18**). The increased TPA values in THF can be ascribed to the increasing contribution of aromatic conformation that would be Möbius strip-like structure. Thus, a small increase in the TPA value in ethyl ether is affected by a small portion of **THF-conformer**. The largest TPA value in DMSO also suggests the predominance of aromatic **DMSO–conformer**, which is conformationally rigid due to the hydrogen bonding between solutes and solvents as mentioned earlier.

**(4) Energy Relaxation Dynamics:** The TA spectra of **toluene–** and **THF–conformers** in this study actually exhibit the typical spectral features of antiaromatic and aromatic expanded porphyrins, respectively. In our TA experiments, antiaromatic expanded porphyrins usually exhibit broad and relatively large ESA bands compared to GSB bands as seen in **toluene–conformer**, while aromatic expanded porphyrins show sharp and much stronger GSB bands than its ESA bands as seen in **THF–conformer**. We suppose that a certain selection rule involved in the excited-states will govern this trend with focusing on the vibrational energy relaxation process observed in TA spectra of **toluene–conformer**. The broad ESA signals in TA spectra of **toluene–conformer** showed ultrafast spectral blue-shift with band narrowing during the initial time evolutions, which is presumed to be a signature

of vibrational energy relaxation process occurring in the excited vibrational state manifolds in the lowest electronic excited state ($S_1$). When the excited populations are generated in higher vibrational states, we can intuitively expect additional appearance of absorption bands in lower energy region like hot-band absorption according to Frank-Condon principles which predict the absorption or emission spectra by the vibrational overlap of the initial and final vibrational states. Thus, the absorption spectra become much broader in this situation. This gives us a clue to diagnose the feature of TA spectra in toluene as an evidence of vibrational energy relaxation. On the other hand, in the TA spectra of THF solution there is no symptom of vibrational relaxation processes. We believe that this difference arises from the distinguished electronic structure of **toluene–conformer**. In the vertical excitation transition calculations the antiaromatic form, which is supposed to be **toluene–conformer**, exhibits one-photon forbidden transition at 2252 nm, so called optically dark state, different from **THF–conformer** (aromatic form). Even though the presence of this optically dark state could not be proved by the steady-state absorption spectra (because the transition is one-photon forbidden), the ultrafast energy relaxation dynamics in toluene reflect the existence of this state.

The decay profiles in THF exhibit only one decay time constant of 65 ps with the photoexcitation at B-like state ($S_B$), which is estimated to be the lifetime of Q-like state ($S_Q$) after ultrafast internal conversion from $S_B$ to $S_Q$ states (< 200 fs). In contrast, the decay profiles of **toluene–conformer** show the two time constants of 0.4 and 5 ps with the same photoexcitation at $S_B$ transition. Because the internal conversion from $S_B$ to $S_Q$ states would be also very fast as in THF, the decay time constant of less than 1 ps in toluene strongly suggests the low-lying state below $S_Q$ transition. In addition, 5 ps time constant is much shorter than the lifetime of 65 ps in THF, which means the energy relaxation of **toluene–conformer** from the lower energy state becomes much faster than that of **THF–conformer** by obeying the energy-gap law. Based on our observations, the degree of aromaticity and π-delocalization in expanded porphyrins change with molecular conformation, seeming to depend on how far p-orbitals overlap smoothly. In this regard, in order to figure out the exact relationships between molecular topology, aromaticity and photophysical properties, further systematic studies on this topic will be studied.

## Summary

In this project, we have investigated the relationship between aromaticity and photophysical properties of various (anti)aromatic porphyrinoids using the spectroscopic techniques and theoretical approaches.

Firstly, the relationship between aromaticity and photophysical properties of [18]/[20]π porphycenes was investigated using various theoretical calculations and spectroscopic measurements. Based on ACID and NICS calculations, π-electron delocalization is more effective in the order of **[18]EtioPc** >**[18]CF$_3$Pc > [20]CF$_3$Pc**, which is in line with the tendency of molecular distortion. Interestingly, we have found that the HOMO-LUMO gap of [20]π porphycene is larger than that of [18]π porphycene, which is in a sharp contrast with those of typical [4n]/[4n+2]π porphyrinoids. Especially, compared with other [4n]π porphyrinoids, [20]π porphycene exhibits unique photophysical behaviors arising from a large HOMO-LUMO energy gap. Consequently, our study demonstrates that the energy difference between LUMO and LUMO+1 levels of aromatic [4n+2]π porphyrinoids is an important factor in determining the electronic nature of their corresponding antiaromatic [4n]π porphyrinoids.

Secondly, [32]heptaphyrin clearly exhibits solvent polarity dependent photophysical properties, which have been revealed by $^1$H NMR, absorption, fluorescence, TA, and TPA measurements. All the measured data indicate that the aromaticity of molecule is changed from antiaromatic to aromatic as the solvent polarity increases in going from toluene to THF and DMSO. According to the quantum mechanical calculations, this feature is mainly ascribed to the conformational changes from antiaromatic Hückel to aromatic Möbius topologies which correspond to the major conformers in toluene and THF, respectively. We could resolve the TA spectra and excited-state lifetimes of the two conformers by varying the excitation wavelength with the global analysis. Particularly, in the TA spectra of toluene solution we have observed the evidence of vibrational energy relaxation process that generates the broad ESA signals at the initial delay time while such phenomena are absent in THF and DMSO solvents. This result is largely associated with the presence of low-lying and optically dark state of **toluene-conformer** and the generation of excess vibrational energy within this state can give us a clue to answer why we have witnessed a consistent trend in the TA spectra of antiaromatic expanded porphyrins distinguished from those of aromatic expanded porphyrins. Finally, this study demonstrates that the spectral features of TA spectra can be utilized to differentiate antiaromatic conformers from aromatic ones in expanded porphyrins.

## References


(1) J. L. Sessler, A. Gebauer, S. J. Weghorn, in *The Porphyrin Handbook*, Vol. 2 (eds. K. M. Kadish, K. M. Smith, R. Guilard), Academic Press, New York, **2000**, ch. 9.

(2) J. L. Sessler, S. Camiolo, P. A. Gale, *Coord. Chem. Rev.* **2003**, *240*, 17.

(3) A. Srinivasan, H. Furuta, *Acc. Chem. Res.* **2005**, *38*, 10.

(4) R. Misra, T. K. Chandrashekar, *Acc. Chem. Res.* **2008**, *41*, 265.

(5) A. Kay, M. Grätzel, *J. Phys. Chem.* **1993**, *97*, 6272.

(6) L. Schmidt-Mende, W. M. Campbell, Q. Wang, K. W. Jolley, D. L. Officer, Md. K. Nazeeruddin, M. Grätzel, *ChemPhysChem* **2005**, *6*, 1253.

(7) M. Stępień, L. Latos-Grażyński, N. Sprutta, P. Chwalisz, L. Szterenberg, *Angew. Chem. Int. Ed.* **2007**, *46*, 7869.

(8) Y. Tanaka, S. Saito, S. Mori, N. Aratani, H. Shinokubo, N. Shibata, Y. Higuchi, Z. S. Yoon, K. S. Kim, S. B. Noh, J. K. Park, D. Kim, A. Osuka, *Angew. Chem. Int. Ed.* **2008**, *47*, 681.

(9) E. Heilbronner, *Tetrahedron Lett.* **1964**, *5*, 1923.

(10) J. Garratt, *Aromaticity*, John Wiley & Sons, Inc., New York, **1986**.

(11) V. I. Minkin, M. N. Glukhotsev, B. Y. Simkin, *Aromaticity and Antiaromaticity: Electronic and Structural Aspects*, John Wiley & Sons, Inc., New York, **1994**.

(12) H. S. Rzepa, *Chem. Rev.* **2005**, *105*, 3697.

(13) R. Herges, *Chem. Rev.* **2006**, *106*, 4820.

(14) K. B. Wiberg, *Chem. Rev.* **2001**, *101*, 1317.

(15) Z. S. Yoon, A. Osuka, D. Kim, *Nature Chem.* **2009**, *1*, 113.

(16) B. Lament, J. Dobkowski, J. L. Sessler, S. J. Weghorn, J. Waluk, *Chem. Eur. J.* **1999**, *10*, 3039.

(17) M. K. Cyranski, T. M. Krygowski, M. Wisiorowski, N. J. R. van E. Hommes, P. von R. Schleyer, *Angew. Chem. Int. Ed.* **1998**, *37*, 177.

(18) H.-E. Song, J. A. Cissell, T. P. Vaid, D. Holten, *J. Phys. Chem. B,* **2007**, *111*, 2138.

# List of Publications

**1. Large Porphyrin Squares from the Self-Assembly of meso-Triazole-Appended L-Shaped meso–meso-Linked $Zn^{II}$–Triporphyrins: Synthesis and Efficient Energy Transfer**
Chihiro Maeda, Pyosang Kim, Sung Cho, Jong Kang Park, Jong Min Lim, Dongho Kim, Josh Vura-Weis, Michael R. Wasielewski, Hiroshi Shinokubo, Atsuhiro Osuka
*Chem. Eur. J.* **2010**, *16(17)*, 5052–5061

**2. A Stable Non-Kekule´ Singlet Biradicaloid from meso-Free 5,10,20,25-Tetrakis(Pentafluorophenyl)-Substituted [26]Hexaphyrin(1.1.1.1.1.1)**
Taro Koide, Ko Furukawa, Hiroshi Shinokubo, Jae-Yoon Shin, Kil Suk Kim, Dongho Kim, Atsuhiro Osuka
*J. Am. Chem. Soc.* **2010**, *132(21),* 7246–7247

**3. Photophysical Properties of N-Confused Hexaphyrins: Effects of Confusion of Pyrrole Rings and Molecular Shape on Electronic Structures**
Jong Min Lim, Jae Seok Lee, Hyun Woo Chung, Hee Won Bahng, Keisuke Yamaguchi, Motoki Toganoh, Hiroyuki Furuta, Dongho Kim
*Chem. Commun.* **2010**, *46(24),* 4357–4359

**4. Aromaticity and Photophysical Properties of Various Topology-Controlled Expanded Porphyrins**
Jae-Yoon Shin, Kil Suk Kim, Min-Chul Yoon, Jong Min Lim, Zin Seok Yoon, Atsuhiro Osuka, Dongho Kim
*Chem. Soc. Rev.* **2010**, *39(8),* 2751–2767

**5. Möbius Antiaromatic Bisphosphorus Complexes of [30]Hexaphyrins**
Tomohiro Higashino, Jong Min Lim, Takahiro Miura, Shohei Saito, Jae-Yoon Shin, Dongho Kim, Atsuhiro Osuka
*Angew. Chem. Int. Ed.* **2010**, *49(29),* 4950 –4954

**6. Multistimuli Two-Color Luminescence Switching via Different Slip-Stacking of Highly Fluorescent Molecular Sheets**
Seong-Jun Yoon, Jong Won Chung, Johannes Gierschner, Kil Suk Kim, Moon-Gun Choi, Dongho Kim, Soo Young Park
*J. Am. Chem. Soc.* **2010**, *132(39)*, 13675–13683

**7. The Self-Assembly and Photophysical Characterization of Tri(Cyclopentaphenanthrene)-Derived Nanoparticles: A Template Free Synthesis of Hollow Colloidosomes.**
Shanmugam Easwaramoorthi, Pyosang Kim, Jong Min Lim, Suhee Song, Honsuk Suh, Jonathan L. Sessler, Dongho Kim
*J. Mater. Chem.* **2010**, *20(43)*, 9684–9694

**8. Molecular-Shape-Dependent Photophysical Properties of meso-β Doubly Linked Zn(II) Porphyrin Arrays and Their Indene-Fused Analogues**
Ji Haeng Heo, Toshiaki Ikeda, Jong Min Lim, Naoki Aratani, Atsuhiro Osuka, Dongho Kim
*J. Phys. Chem. B* **2010**, *114(45)*, 14528–14536

**9. Synthesis and Photophysical Properties of N-Fused Tetraphenylporphyrin Derivatives: Near-Infrared Organic Dye of [18] Annulenic Compounds**
Shinya Ikeda, Motoki Toganoh, Shanmugam Easwaramoorthi, Jong Min Lim, Dongho Kim, Hiroyuki Furuta
*J. Org. Chem.* **2010**, *75(24)*, 8637–8649

**10. Characterization of Ultrafast Intramolecular Charge Transfer Dynamics in Pyrenyl Derivatives: Systematic Change of the Number of Peripheral N,N-Dimethyaniline Substituents**
Jooyoung Sung, Pyosang Kim, Yoen Ok Lee, Jong Seung Kim, Dongho Kim
*J. Phys. Chem. Lett.* **2011**, *2(7),* 818–823

**11. Conformation Dynamics of Non-, Singly- and Doubly-N-Fused [28]Hexaphyrins Revealed by Photophysical Studies**
Jong Min Lim, Mitsunori Inoue, Young Mo Sung, Masaaki Suzuki, Tomohiro Higashino, Atsuhiro Osuka, Dongho Kim
*Chem. Commun*. **2011**, *47(13)*, 3960–3962

**12. Excited-State Energy Relaxation Dynamics of Triply Linked Zn(II) Porphyrin Arrays**
Pyosang Kim, Toshiaki Ikeda, Jong Min Lim, Jaeheung Park, Manho Lim, Naoki Aratani, Atsuhiro Osuka, Dongho Kim
*Chem. Commun*. **2011**, *47(15)*, 4433–4435

**13. Synthesis and Properties of Boron(III)-Coordinated Subbacteriochlorins**
Shin-ya Hayashi, Eiji Tsurumaki, Yasuhide Inokuma, Pyosang Kim, Young Mo Sung, Dongho Kim, Atsuhiro Osuka
*J. Am. Chem. Soc.* **2011**, *133(12),* 4254–4256

**14. Ultrafast Intramolecular Energy Relaxation Dynamics of Benzoporphyrins: Influence of Fused Benzo Rings on Singlet Excited States**
Pyosang Kim, Jooyoung Sung, Hiroki Uoyama, Tetsuo Okujima, Hidemitsu Uno, Dongho Kim
*J. Phys. Chem. B* **2011**, *115(14*), 3784–3792

**15. Oxocyclohexadienylidene-Substituted Subporphyrins**
Shin-ya Hayashi, Jooyoung Sung, Young Mo Sung, Yasuhide Inokuma, Dongho Kim, Atsuhiro Osuka
*Angew. Chem. Int. Ed.***2011***, 50(14),* 3253 –3256

**16. Solvent Dependent Aromatic versus Antiaromatic Conformational Switching in meso-(Heptakis)pentafluorophenyl [32]Heptaphyrin**
Min-Chul Yoon, Jae-Yoon Shin, Jong Min Lim, Shohei Saito, Tomoki Yoneda, Atsuhiro Osuka, Dongho Kim
*Chem. Eur. J.* **2011***, (accepted)*

**17. Investigation of Aromaticity and Photophysical Properties in [18]/[20]π Porphycene Derivates**
Kil Suk Kim, Young Mo Sung, Takashi Matsuo, Takashi Hayashi, Dongho Kim
*Chem. Eur. J.* **2011***, (accepted)*

**DD882:** As a separate document, please complete and sign the inventions disclosure form.

This document may be as long or as short as needed to give a fair account of the work performed during the period of performance. There will be variations depending on the scope of the work. As such, there are no length or formatting constraints for the final report. Include as many charts and figures as required to explain the work. A final report submission very similar to a full length journal article will be sufficient in most cases.